

Improved Hydrogen Monitoring Properties Based on p-NiO/n-SnO₂ Heterojunction Composite Nanofibers

Zhaojie Wang,[†] Zhenyu Li,[†] Jinghui Sun,[‡] Hongnan Zhang,[†] Wei Wang,[†] Wei Zheng,[†] and Ce Wang*,[†]

Alan G. MacDiarmid Institute, Jilin University, Changchun 130012, P. R. China, and Norman Bethune College of Medicine, Jilin University, Changchun 130000, P. R. China

Received: October 20, 2009; Revised Manuscript Received: February 11, 2010

Here we demonstrate the preparation and improved hydrogen monitoring properties based on p-NiO/n-SnO₂ heterojunction composite nanofibers via the electrospinning technique and calcination procedure. NiO/SnO₂ heterojunction composite nanofibers were spin-coated on the ceramic tube with a pair of Au electrodes for the detection of hydrogen. Extremely fast response–recovery behavior (~3 s) has been obtained at the operable temperature of 320 °C, based on our gas sensor, with the detection limit of approximate 5 ppm H₂. The role of the addition of NiO into the SnO₂ nanofibers and the sensing mechanism has also been discussed in this work.

1. Introduction

Taking the advantages of high calorific value, abundance, nonpollution, and being lightweight, hydrogen (H₂) has been acting as one of the most potent energy vectors and used more and more in daily life and industrial areas.^{1,2} However, as a colorless, odorless, and extremely flammable gas with a lower explosive limit of 4% in air (40 000 ppm),³ massive hydrogen usage requires, in addition to safe control systems, a fast and sensitive H₂ monitor. The main research interest is focus on lowering the response time of the sensor to the leaking hydrogen, and up to now, the following strategies have been aimed at reducing the dimension of sensitive materials.^{4–8} For instance, the hydrogen sensor based on Pd nanocluster film with a response time as short as 70 ms has been reported.⁹ However, it is an expensive and complex multiprocedure to fabricate such nanodevices.

The electrospinning technique for fabricating one-dimensional (1D) metal oxides nanofibers has emerged as an alternative for gas sensing, and at present, there is increasing interest in it. Until now, many gas sensors based on TiO₂,¹⁰ ZnO,¹¹ Fe₂O₃,¹² and In₂O₃¹³ nanofibers have been developed via electrospinning. Among various oxides, SnO₂ is one of the most attractive and commercial materials for semiconductor gas sensor, such as ethanol,¹⁴ acetone,^{15,16} and toluene.¹⁷ However, gas sensing performances based on P–N heterojunction composite nanofibers have been not explored yet.

Herein, NiO, as the other component, was implanted into the SnO₂ nanofibers via the electrospinning technique and calcination process. NiO is a p-type semiconductor with an energy gap of about 4.2 eV¹⁸ and easily forms heterojunctions with SnO₂, which is an n-type semiconductor with an energy gap of about 3.5 eV.¹⁹ The introduction of NiO leads to formation of a barrier mechanism of conductivity.²⁰ The electrical barrier can be originated by p–n junction formation between the grains of n-SnO₂ and p-NiO. When they are brought together to form a p–n contact, they show sensitivity to reducing gases.^{21–23} In

the present work, excellent H₂ sensing properties such as high sensitivity and fast response–recovery behavior have been observed at 320 °C based on SnO₂ nanofibers containing 4.11 mol % NiO. These results demonstrate a promising approach in development and realization of a low-cost and high-performance hydrogen sensor.

2. Experiment

2.1. Chemicals. Ethanol (>95%), *N,N*-dimethyl formamide (>95%), and SnCl₂·2H₂O were purchased from Tianjin Chemical Company. Poly(vinyl pyrrolidone) (PVP, *M*_w = 1 300 000) was purchased from Aldrich. NiCl₂·6H₂O was purchased from Sinopharm Chemical Reagent Co., Ltd. All chemicals were used as received without any further purification.

2.2. Preparation and Characterization of Nanofibers. p-NiO/n-SnO₂ composite nanofibers were fabricated by electrospinning followed by calcination. In a typical procedure, 0.36 g of SnCl₂·2H₂O was mixed with 4.4 g of DMF and 4.4 g of ethanol in a glovebox under vigorous stirring for 10 min. Subsequently, 0.8 g of PVP and a suitable amount (0.0036, 0.0108, 0.036, or 0.054 g) of NiCl₂·6H₂O was added into the above solution under vigorous stirring for 30 min. Then the mixture was loaded into a glass syringe and connected to high-voltage power supply. Ten kilovolts was provided between the cathode (a flat foil) and anode (syringe) at a distance of 20 cm. Finally, calcination (600 °C in air for 5 h) was used to treat the as-spun nanofibers to remove the organic constituent of PVP and to convert the precursor to p-NiO/n-SnO₂ composite nanofibers. The pure SnO₂ nanofibers were also obtained with no addition of NiCl₂·6H₂O.

Nanofibers were characterized by means of scanning electron microscope (SEM, SSX-550, Shimadzu), transmission electron micrographs (TEM, Hitachi S-570), and X-ray diffraction (XRD, Scintag XDS 2000 diffractometer with a Cu K α radiation). Analysis of the X-ray photoelectron spectra (XPS) was performed on an ESCLAB MKII using Al as the exciting source.

2.3. Preparation of the Sensor Device. The as-prepared p-NiO/n-SnO₂ composite nanofibers were mixed with deionized water in a weight ratio of 100:25 to form a paste. The paste was coated onto a ceramic tube on which a pair of gold electrodes was previously printed, and then a Ni–Cr heating

* To whom correspondence should be addressed. E-mail: cwang@jlu.edu.cn. Tel.: +86 431 85168292. Fax: +86 431 85168292.

† Alan G. MacDiarmid Institute.

‡ Norman Bethune College of Medicine.

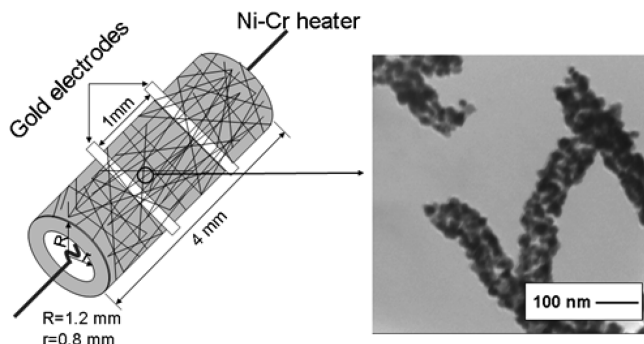


Figure 1. Schematic illustration of the fabricated device structure for the H₂ sensing measurement and the corresponding TEM image of the 4.11 mol % NSNFs.

wire was inserted in the tube to form a side-heated gas sensor as shown in Figure 1. The geometry and dimension of the sensor have also been marked in the scheme in Figure 1. Gas sensing properties were measured using a static test system. Saturated target vapor was injected into a glass test chamber (about 20 L in volume) by a syringe through a rubber plug. After being fully mixed with air (relative humidity was about 25%), the sensor was put into the test chamber. When the sensitivity reached a constant value, the sensor was taken out to recover in air. The electrical properties of sensors were measured by the CGS-1 intelligent test system (Beijing Elite Tech Co. Ltd., China). The sensor response (S) was measured between 260 and 380 °C by comparing the resistance of the sensor in dry synthetic air (R_a) with that in target gases (R_g). The time taken by the sensor to achieve 90% of the total resistance change was defined as the response time in the case of adsorption or the recovery time in the case of desorption.

3. Results and Discussion

3.1. Morphological and Structural Characteristics of the Products.

Figure 2 shows the SEM images of the pure SnO₂

nanofibers and as-prepared p-NiO/n-SnO₂ composite nanofibers (NSNFs) with different molar ratio contents of NiO, respectively. It can be seen that after calcinations at 600 °C, the nanofibers remain intact, indicating a good quantity of the NSNFs, with the average diameter of the nanofibers ranging from 100 to 200 nm as can be obtained via our method. During the thermal treatment, PVP was removed, resulting in a rough surface occurring and the surface area increasing obviously as illustrated by the TEM image in Figure 1. It also shows that the 4.11 mol % NSNFs are indeed composed of many interconnected grains of around 20 nm in size. The similar morphology and structures are observed as well for the pure SnO₂ nanofibers and NSNFs with 1.37, 6.85, and 13.7 mol % NiO.

XRD is used to examine the crystal structure of pure SnO₂ nanofibers and NSNFs. All the strong diffraction peaks in Figure 3 can be perfectly indexed as the tetragonal rutile structure for SnO₂ (JCPDS 41-1445). Compared with SnO₂, the diffraction peaks of NiO can hardly be observed, indicating a high solubility of NiO in SnO₂. The high solubility is reasonable, considering their same ionic radius (0.69 Å). No other characteristic peaks for impurity are observed. To further illuminate the surface composition and the chemical state of the elements existing in the as-prepared NSNFs, we conducted XPS studies, and the spectra are illustrated in Figure 4. The Ni2p signal can be deconvoluted into several peaks in Figure 4 a. The binding energies at 855.6 and 861.2 eV are attributed to the Ni2p_{3/2} peaks, and the 874.1 and 879.1 eV peaks are attributed to Ni2p_{1/2}.²⁴ The Ni2p_{3/2} peaks are assigned to Ni(II) ions in the NSNFs samples. The high peak at 855.6 was attributed to NiO₅ or Ni²⁺ in pyramidal symmetry according to the experimental results and theoretical calculation of Soriano et al.²⁵ The spin-orbit components (3d_{3/2} and 3d_{5/2}) of the Sn3d peak are both observed at approximately 495.2 and 486.7 eV as shown in Figure 4b, corresponding to Sn⁴⁺ in a tetragonal rutile structure.²⁶ Similarly, the O1s XPS spectrum in Figure 4c shows a narrow peak with a binding energy of 530.6 eV and high

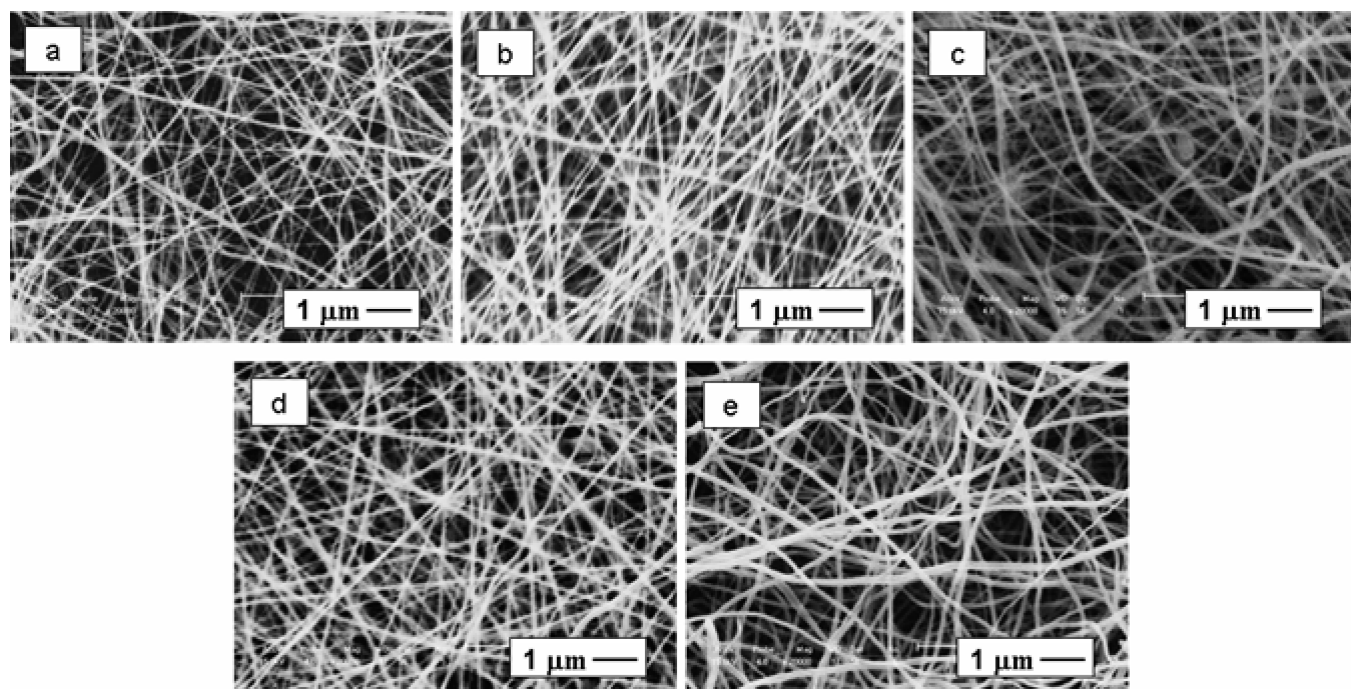


Figure 2. SEM images of (a) pure SnO₂ nanofibers and (b) 1.37 mol %, (c) 4.11 mol %, (d) 6.85 mol %, and (e) 13.7 mol % NiO–SnO₂ composite nanofibers.

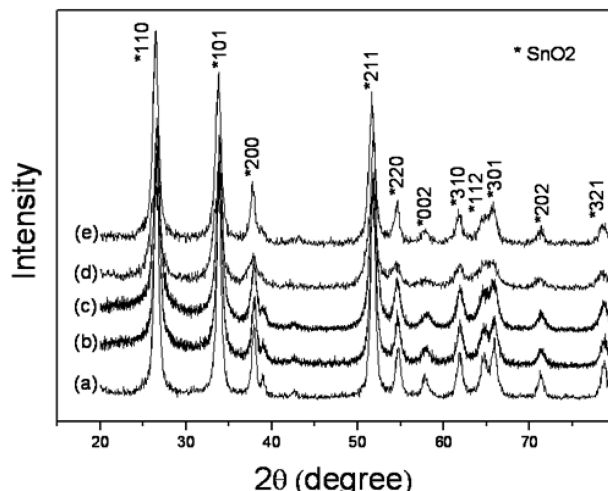


Figure 3. XRD patterns of (a) pure SnO_2 nanofibers and (b) 1.37 mol %, (c) 4.11 mol %, (d) 6.85 mol %, and (e) 13.7 mol % $\text{NiO}-\text{SnO}_2$ composite nanofibers.

symmetry. All of these results give the insight that the nanofibers are composed of NiO and SnO_2 .

3.2. Sensing Properties. The influence of the addition of NiO in NSNFs on the sensitivity for the hydrogen detecting was studied first as shown in Figure 5. In contrast to the pure SnO_2 nanofibers, the introduction of NiO can enhance the sensitivity to 100 ppm H_2 at 320 °C dramatically. Especially when the intermingled quantity of NiO is 4.11 mol %, its response is more than three times that of pure SnO_2 nanofibers, which suggests the 4.11 mol % NSNFs to be an optimized sample.

The optimal operating temperature of the NSNFs sensors for detecting H_2 is an important issue, and it was obtained by performing the gas-sensing experiments at different temperatures. Before being exposed to the target gas, each sensor was stabilized for 2 h at the working temperature. Figure 6 presents responses to 100 ppm of H_2 for pure SnO_2 nanofibers and the 4.11 mol % NSNFs samples. The response increases and reaches its maximum at 320 °C and then decreases rapidly with increasing temperatures. In summary, compared with pure SnO_2 nanofibers sensor, the 4.11 mol % NSNFs sensor exhibits the highest response at 320 °C, which indicates that the addition of NiO is beneficial to the H_2 sensing.

The concentration dependence of pure SnO_2 nanofibers and NSNFs was investigated in the range of 5–20 000 ppm H_2 , and the plots of the gas response against the gas concentration are shown in Figure 7. As for the 4.11 mol % NSNFs, the results clearly indicate that even the lowest concentration of H_2 , i.e., 5 ppm, can be detected with response value >3, which is a hopeful and acceptable response value. The response increases rapidly with increasing H_2 concentration at first (below 10 000 ppm). Above 10 000 ppm, the response slowly increases with increasing H_2 concentration, which indicates that the sensor becomes more or less saturated. Finally, the sensor reaches saturation after exposure to more than 15 000 ppm, which means that no more active sites were available to react with new H_2 molecules when the concentration of H_2 is increased. Although a similar trend was also observed for pure SnO_2 nanofibers, the responses are much weaker.

In order to clarify the advantages of the NSNFs in the sensor response to hydrogen, we quantitatively compare our studies with previous works using SnO_2 and NiO for hydrogen sensing. The comparison of sensor response at different hydrogen

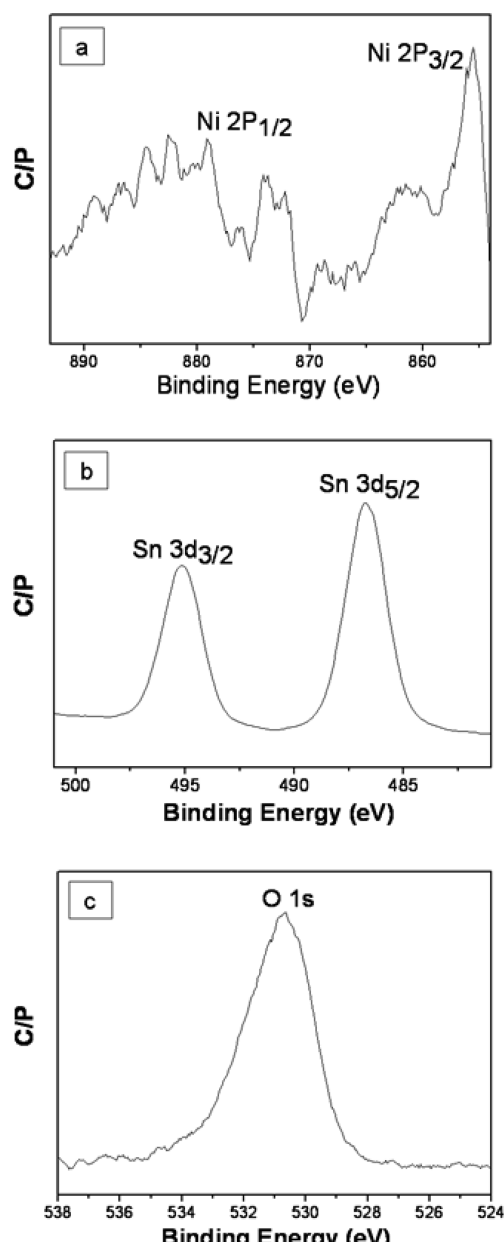


Figure 4. XPS spectra of (a) $\text{Ni}2\text{p}$, (b) $\text{Sn}3\text{d}$, and (c) $\text{O}1\text{s}$ electron binding energies of the 4.11 mol % $\text{NiO}-\text{SnO}_2$ composite nanofibers.

concentrations of various metal oxides for hydrogen sensing is summarized in Table 1. However, some data of the sensor response from the literature, such as ref 27, may not be expressed as $S = R_a/R_g$. In order to give convincing comparative data, we have made a suitable transformation to them. Thus, the sensor responses from other literature in Table 1 are comparable. Accordingly, these results definitely show that the NSNFs gas sensor has achieved much better sensing results than that of other metal oxides for hydrogen sensing.

It is well-known that response and recovery characteristics are important for evaluating the performances of hydrogen sensors. To investigate the response–recovery behaviors of 4.11 mol % NSNFs sensor, the sensor was sequentially exposed to 5, 50, 100, 500, and 1000 ppm H_2 at 320 °C. The sensor exhibits high response and fast response and recovery to H_2 , which is shown in Figure 8. The response and recovery times are very short ($\sim 3\text{s}$) and change slightly with changing H_2 concentration.

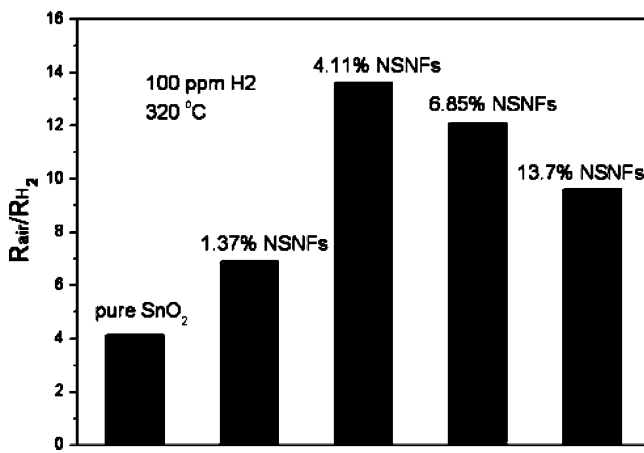


Figure 5. Responses of the sensors to 100 ppm H₂ at 320 °C.

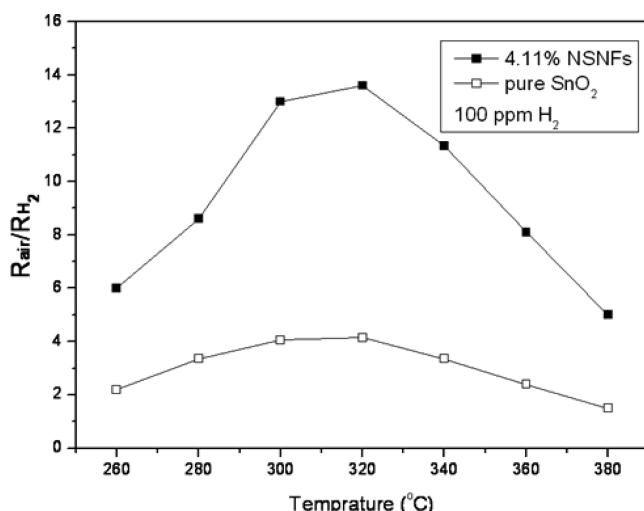


Figure 6. Responses of pure SnO₂ and 4.11 mol % NSNFs to 100 ppm H₂ as a function of operating temperature.

3.3. Research in Sensing Mechanism. For SnO₂-based sensing materials, the high performance can be explained by the space-charge layer mode.³² The change in resistance is primarily caused by the adsorption and desorption of the target gas molecules on the surface of the sensing structure.³³ As tin oxide is exposed to air, oxygen molecules will be adsorbed on the oxide surface and then extract electrons in the bulk to become oxygen ions, leading to a narrow conduction channel. Consequently, depletion layers are formed in the surface area of the SnO₂ nanofibers with an aligned arrangement, causing the carrier concentration to decrease and leading to the high resistance of the sensor. When the SnO₂ nanofibers are exposed to H₂, the hydrogen molecules will react with the adsorbed ions, and then the conduction channel becomes wider. The trapped electrons are released back to the conduction band, and then the carrier concentration of SnO₂ will increase.

By adding NiO, p-n heterojunction is formed at the interface between NiO and SnO₂. While oxygen-deficient SnO₂ shows n-type conductivity by electrons, oxygen-excess NiO shows p-type conductivity by holes. Sintered gas sensors are composed of a mixture of NiO and SnO₂, and thus, NiO is dispersed here and there in a sensor as shown in Figure 9a. In this case, in an oxidizing atmosphere a thicker charge depletion layer is formed near the grain surface of SnO₂ as a p-n junction. The electrons associated with these charged species are drawn from the conduction band of the bulk material, leading to an increase in

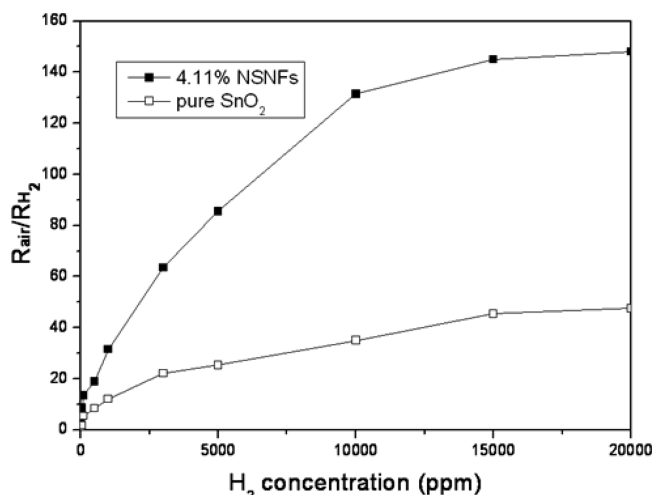


Figure 7. Responses to H₂ concentration in the range from 5 to 20 000 ppm for pure SnO₂ and 4.11 mol % NSNFs sensors.

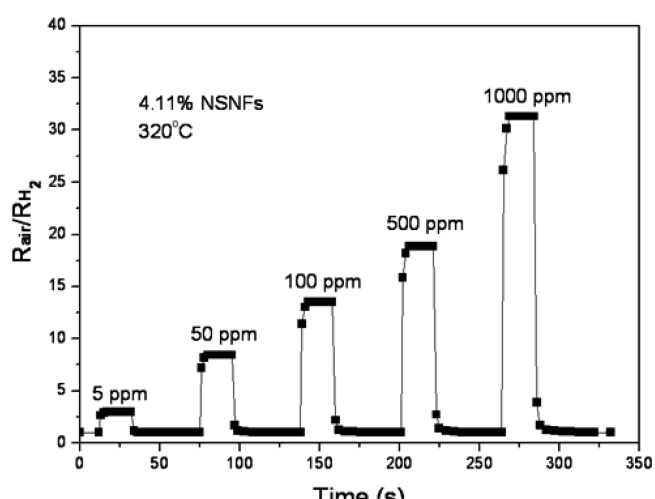


Figure 8. Response and recovery characteristic curves of the sensor based on 4.11 mol % NSNFs to H₂ in the range of 5–1000 ppm at 320 °C.

resistance. H₂ increases the number of electrons in the SnO₂ and decreases the concentration of holes in NiO; therefore, the thinner depletion layer thickness leads to lower resistance. An energy band model for a CuO-SnO₂,³⁴ CuO-ZnO,³⁵ NiO-ZnO³⁶ heterocontact has been proposed that may be similar to the NiO/SnO₂ system. As shown in Figure 9b, the contact between n- and p-type semiconductors results in band bending in the depletion layers on either side of the physical interface to accommodate the equalization of the Fermi levels. The distribution and extent of electrically active contacts between the two phases is also the key parameter in describing the active junction where sensing can take place.³⁷

Overall, the addition of p-type NiO enhanced the hydrogen adsorption kinetics thereby increasing the sensitivity of the heterocontact sensor. The reaction near the heterocontact interface can be simply written as



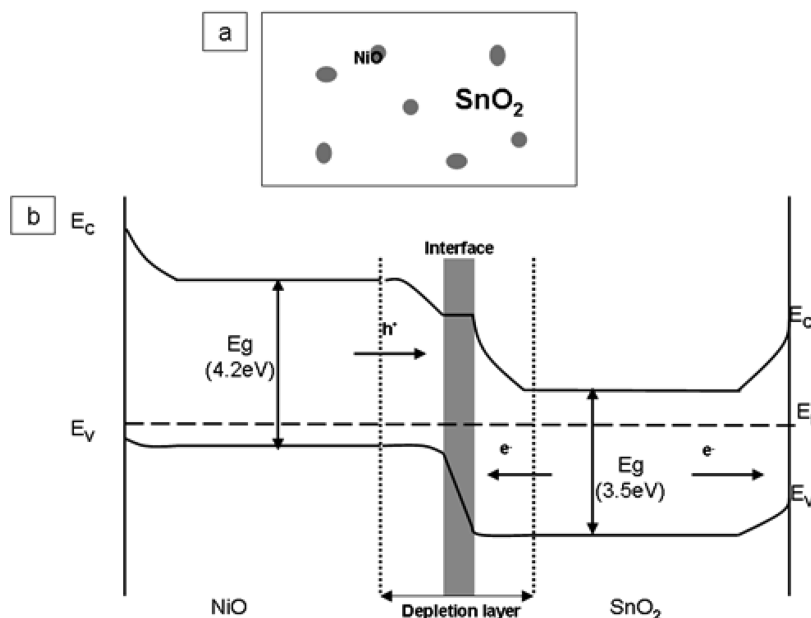


Figure 9. (a) Scheme showing that NiO is randomly dispersed in SnO₂. (b) Proposed ideal band structure for a p-NiO/n-SnO₂ heterojunction. E_c, lower level of conduction band; E_F, Fermi level; E_v, upper level of valence band.

TABLE 1: Comparison of the Sensor Response to Hydrogen with Different Concentrations at Individual Operating Temperature

	5 ppm	10 ppm	500 ppm	1000 ppm	1%	2%	3%	T/°C
NiO/SnO ₂ nanofibers	3		19	32.5	131.43	148	~150	320
SnO ₂ nanofibers	1		8.4	12.15	35	47.5	~50	320
SnO ₂ nanowire ²⁷		1.4		4.25				300
SnO ₂ nanorod ²⁷			1.4					300
SnO ₂ nanobelt ²⁸							1.6	80
SnO ₂ film ^{29,30}		1.18						300
Pt/NiO film ³¹							3.5	140

The forward resistance was further decreased in the presence of hydrogen due to the enhancement of reaction 2.³⁸

Besides the high sensitivity, the extremely fast response and recovery behavior can be attributed to the 1D nanostructure of NSNFs. It can facilitate fast mass transfer of the hydrogen molecules to and from the interaction region as well as improve the rate for charge carriers to transverse the barriers induced by molecular recognition along the fibers.³⁹ Therefore, the excellent H₂ sensing properties of NSNFs sensor are ascribed to the cooperative effect of all the above-mentioned factors.

4. Conclusions

p-NiO/n-SnO₂ heterojunction composite nanofibers have been fabricated via the electrospinning technique and calcination process. The as-prepared samples were evaluated for their gas sensing properties toward H₂, and better responses were observed than for the pure SnO₂ nanofibers. A maximum response value of 13.6 and extremely fast response–recovery behavior are obtained for 100 ppm H₂ detection at 320 °C. These results demonstrate a promising approach in development and realization of a low-cost and high-performance hydrogen sensor.

Acknowledgment. The work has been supported by National 973 Project (No. 2007CB936203 and S2009061009), NSF China (No. 50973038), and National 863 Project (No. 2007AA03Z324).

References and Notes

- (1) Dunn, S. *Int. J. Hydrogen Energy* **2002**, *27*, 235.
- (2) Huang, J. R.; Hsu, W. C.; Chen, Y. J.; Wang, T. B.; Lin, K. W.; Chen, H. I.; Liu, W. C. *Sens. Actuators, B* **2006**, *117*, 151.
- (3) Hotovy, I.; Huran, J.; Siciliano, P.; Capone, S.; Spiess, L.; Rehacek, V. *Sens. Actuators, B* **2004**, *103*, 300.
- (4) Wang, G. X.; Gou, X. L.; Horvat, J.; Park, J. *J. Phys. Chem. C* **2008**, *112*, 15220.
- (5) Wang, B.; Zhu, L. F.; Yang, Y. H.; Xu, N. S.; Yang, G. W. *J. Phys. Chem. C* **2008**, *112*, 6643.
- (6) Virji, S.; Kaner, R. B.; Weiller, B. H. *J. Phys. Chem. B* **2006**, *110*, 22266.
- (7) Baselt, D. R.; Fruhberger, B.; Klaassen, E.; Cemalovic, S.; Britton, C. L., Jr.; Patel, S. V.; Mlsna, T. E.; McCorkle, D.; Warmack, B. *Sens. Actuators, B* **2003**, *88*, 120.
- (8) DiMeo, F., Jr.; Chen, I. S.; Chen, P.; Neuner, J.; Roerhl, A.; Welch, J. *Sens. Actuators, B* **2006**, *117*, 10.
- (9) Xu, T.; Zach, M. P.; Xiao, Z. L.; Rosenmann, D.; Welp, U.; Kwok, W. K.; Crabtree, G. W. *Appl. Phys. Lett.* **2005**, *86*, 203104.
- (10) Zhang, H. N.; Li, Z. Y.; Liu, L.; Wang, C.; Wei, Y.; MacDiarmida, A. G. *Talanta* **2009**, *79*, 953.
- (11) Wang, W.; Huang, H. M.; Li, Z. Y.; Zhang, H. N.; Wang, Y.; Zheng, W.; Wang, C. *J. Am. Ceram. Soc.* **2008**, *91*, 3817.
- (12) Zheng, W.; Li, Z. Y.; Zhang, H. N.; Wang, W.; Wang, Y.; Wang, C. *Mater. Res. Bull.* **2009**, *44*, 1431.
- (13) Zheng, W.; Lu, X. F.; Wang, W.; Li, Z. Y.; Zhang, H. N.; Wang, Y.; Wang, Z. J.; Wang, C. *Sens. Actuators, B* **2009**, *142*, 61.
- (14) Song, X. F.; Wang, Z. J.; Liu, Y. B.; Wang, C.; Li, L. J. *Nanotechnology* **2009**, *20*, 075501.
- (15) Patil, S. B.; Patil, P. P.; More, M. A. *Sens. Actuators, B* **2007**, *125*, 126.
- (16) Jia, Y.; He, L. F.; Guo, Z.; Chen, X.; Meng, F. L.; Luo, T.; Li, M. Q.; Liu, J. *H. J. Phys. Chem. C* **2009**, *113*, 9581.

- (17) Qi, Q.; Zhang, T.; Liu, L.; Zheng, X. *J. Sens. Actuators, B* **2009**, *137*, 471.
- (18) Cantalinia, C.; Postb, M.; Busoc, D.; Guglielmic, M.; Martuccic, A. *Sens. Actuators, B* **2005**, *108*, 184.
- (19) Hoa, N. D.; Quy, N. V.; Cho, Y. S.; Kim, D. *Phys. Status Solidi A* **2007**, *204*, 1820.
- (20) Rumenantseva, M. N.; Gaskov, A. M.; Ryabova, L. I.; Senateur, J. P.; Chenevier, B.; Labreau, M. *J. Mater. Sci. Eng.* **1996**, *41*, 331.
- (21) Vasiliev, R. B.; Rumenantseva, M. N.; Yakovlev, N. V.; Gaskov, A. M. *Sens. Actuators, B* **1998**, *50*, 186.
- (22) Tang, H. X.; Yan, M.; Zhang, H.; Li, S. Z.; Ma, X. F.; Wang, M.; Yang, D. R. *Sens. Actuators, B* **2006**, *114*, 910.
- (23) Jung, S. J.; Yanagida, H. *Sens. Actuators, B* **1996**, *37*, 55.
- (24) Zhao, B.; Ke, X. K.; Bao, J. H.; Wang, C. L.; Dong, L.; Chen, Y. W.; Chen, H. L. *J. Phys. Chem. C* **2009**, *113*, 14440.
- (25) Soriano, L.; Preda, I.; Gutierrez, A.; Palacián, S. *Phys. Rev. B* **2007**, *75*, 233417.
- (26) Hafaiedh, I.; Helali, S.; Cherif, K.; Abdelghani, A.; Tournier, G. *Mater. Sci. Eng., C* **2008**, *28*, 584–587.
- (27) Wang, B.; Zhu, L. F.; Yang, Y. H.; Xu, N. S.; Yang, G. W. *J. Phys. Chem. C* **2008**, *112*, 6643.
- (28) Kind, L. H.; Messer, B.; Kim, F.; Yang, P. *Angew. Chem., Int. Ed.* **2002**, *41*, 2405.
- (29) Wheeler, M. C.; Tiffany, J. E.; Walton, R. M.; Cavicchi, R. E.; Semancik, S. *Sens. Actuators, B* **2001**, *77*, 167.
- (30) Cavicchi, R. E.; Suehle, J. S.; Kreider, K. G.; Shomaker, B. L.; Small, J. A.; Gaitan, M.; Chaparala, P. *Appl. Phys. Lett.* **1995**, *66*, 812.
- (31) Shin, W.; Imai, K.; Izu, N.; Murayama, N. *Jpn. J. Appl. Phys.* **2001**, *40*, 1232.
- (32) Hafaiedh, I.; Helali, S.; Cherif, K.; Abdelghani, A.; Tournier, G. *Mater. Sci. Eng., C* **2008**, *28*, 584.
- (33) Gopel, W.; Schierbaum, K. D. *Sens. Actuators, B* **1995**, *26–27*, 1.
- (34) Tamaki, J.; Maekawa, T.; Miura, N.; Yamazoe, N. *Sens. Actuators, B* **1992**, *9*, 205.
- (35) Nakamura, Y.; Yoshioka, N.; Miyayama, M.; Yanagida, H.; Tsurutani, T.; Nakamura, Y. *J. Electrochem. Soc.* **1990**, *137*, 940.
- (36) Marra, R. A.; Nakamura, Y.; Fujitsu, S.; Yanagida, H. *J. Am. Ceram. Soc.* **1986**, *69*, c-143.
- (37) Leach, C.; Ling, Z.; Freer, R. *Scr. Mater.* **2000**, *42*, 1083.
- (38) Aygün, S.; Cann, D. *Sens. Actuators, B* **2005**, *106*, 837.
- (39) Li, Z. Y.; Zhang, H. N.; Zheng, W.; Wang, W.; Huang, H. M.; Wang, C.; MacDiarmid, A. G.; Wei, Y. *J. Am. Chem. Soc.* **2008**, *130*, 5036.

JP9100202